Supporting Information For

A rapid *in-situ* synthesis of bioinspired nanoflowers on a microfluidic dipstick for point-of-care diagnosis of normoglycemic glycosuria

*Saminu Abdullahi, Mohamed H. I. Gama, Mubashir Ali, Zhu Yang, Han Yujia, Jinzhen Li, Yuhang Liu, Xuzhong Wang, and Zedong Nie**

1. Optimization of enzymes and chromogenic substrate concentrations

The concentration of enzymes and chromogenic substrate plays a crucial role in determining the efficiency of the glucose sensing system. To achieve optimal glucose detection performance, the concentrations of key enzymatic components, glucose oxidase (GOx), horseradish peroxidase (HRP), and the chromogenic substrate (TMB), were systematically optimized. The optimization process was carried out in a stepwise manner to ensure accurate assessment of each component's impact on the overall signal response.

The optimization of GOx concentration was conducted by systematically evaluating its effect on the colorimetric response while maintaining HRP at a fixed concentration of 1.0 mg/mL. This approach allowed for the assessment of GOx's direct influence on the reaction without interference from HRP variations. As shown in Fig. S1a, increasing GOx concentration from 0.1 mg/mL to 1.0 mg/mL results in a significant rise in signal change (ΔR), indicating enhanced catalytic activity due to a higher availability of glucose oxidation sites. This increase in reaction

efficiency directly correlates with the generation of hydrogen peroxide (H_2O_2), which is essential for subsequent HRP-catalyzed oxidation of TMB. However, beyond 1.0 mg/mL GOx concentration, the signal plateaus, indicating that the reaction reaches a saturation point where additional GOx does not contribute to increased catalytic activity. This effect could be attributed to steric hindrance, where excessive enzyme molecules crowd the reaction space, potentially limiting substrate diffusion and reducing overall efficiency. Additionally, enzyme aggregation at high concentrations may lead to partial deactivation, further diminishing any potential signal enhancement. Based on these findings, 1.0 mg/mL GOx was identified as the optimal concentration and was subsequently used for HRP optimization.

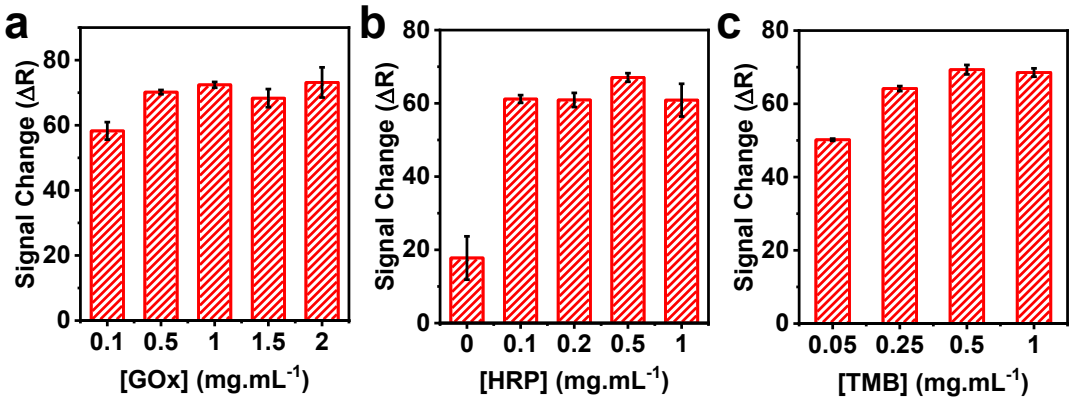

Fig. S1 Effect of enzyme and chromogenic substrate concentrations on glucose detection sensitivity. a showing the effect of increasing GOx concentration on the colorimetric response. **b** evaluating the role of HRP in catalyzing the colorimetric reaction. **c** determining the optimal amount of chromogenic substrate for maximizing signal intensity. Error bars represent the standard deviation (SD) from n = 3 independent measurements.

With the optimal GOx concentration fixed at 1.0 mg/mL, the effect of HRP concentration on the signal response was systematically analyzed, as depicted in Fig. S1b. The effect of HRP

concentration was then analyzed while keeping GOx constant at its optimal level, allowing the specific contribution of HRP to be evaluated. A steady increase in signal is observed as HRP concentration rises from 0.0 mg/mL to 0.1 mg/mL, confirming its essential role in catalyzing TMB oxidation. However, beyond 0.1 mg/mL, no significant variation in the signal response is observed, even at 1.0 mg/mL HRP. This indicates that higher HRP concentrations do not enhance performance, likely due to sufficient catalytic activity being achieved at lower enzyme levels. Given this trend, 0.1 mg/mL HRP was determined to be the optimal concentration, along with 1.0 mg/mL GOx, for subsequent hybrid Nanoflower (HNF) synthesis and paper strip functionalization. Maintaining this balanced enzyme ratio ensures optimal catalytic efficiency while minimizing unnecessary enzyme consumption.

Beyond enzyme concentrations, the effect of TMB concentration was also investigated to optimize the chromogenic signal response, as shown in Fig. S1c. TMB levels were systematically varied between 0.05 mg/mL to 1.0 mg/mL to identify the concentration that maximized signal intensity while minimizing background noise. The signal response increases with TMB concentration, reaching saturation at 0.5 mg/mL, beyond which no further enhancement is observed. This indicates that higher TMB concentrations do not significantly improve colorimetric response and may instead contribute to background noise. Based on this trend, 0.5 mg/mL TMB was selected as the optimal concentration for subsequent experiments to ensure a high signal-to-noise ratio.

These findings emphasize the importance of precisely balancing the enzyme and substrate concentrations to achieve optimal glucose detection performance. By fine-tuning the enzyme-to-substrate ratio, the system achieves a robust and reliable colorimetric response, making it well-suited for practical applications such as urine glucose monitoring.

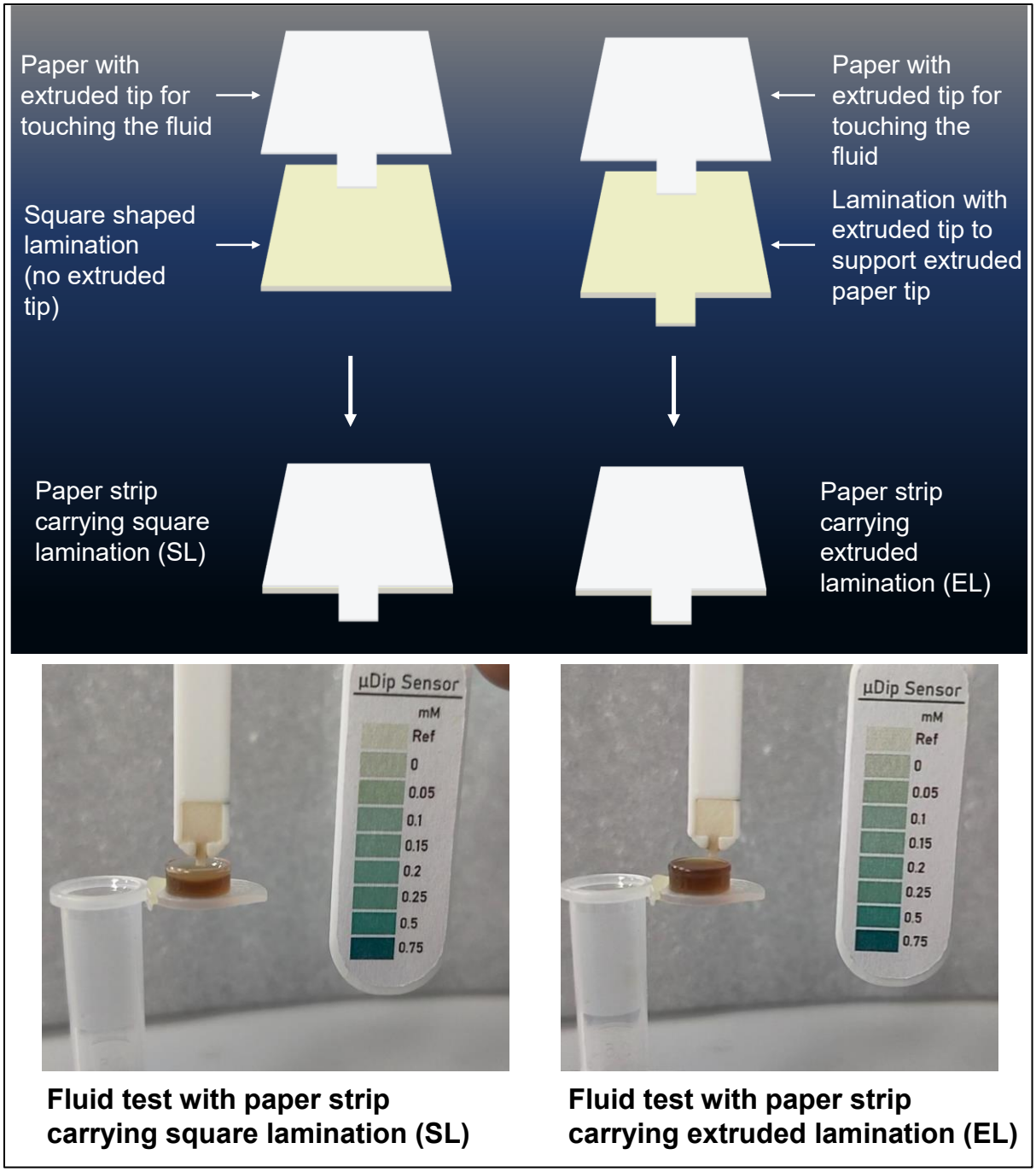

Fig. S2 Comparison of square-laminated (SL) and extruded-laminated (EL) paper strips for fluid uptake. Highlighting the role of lamination in supporting the extruded paper tip during dip-and-detect with the hybrid µDip sensor.

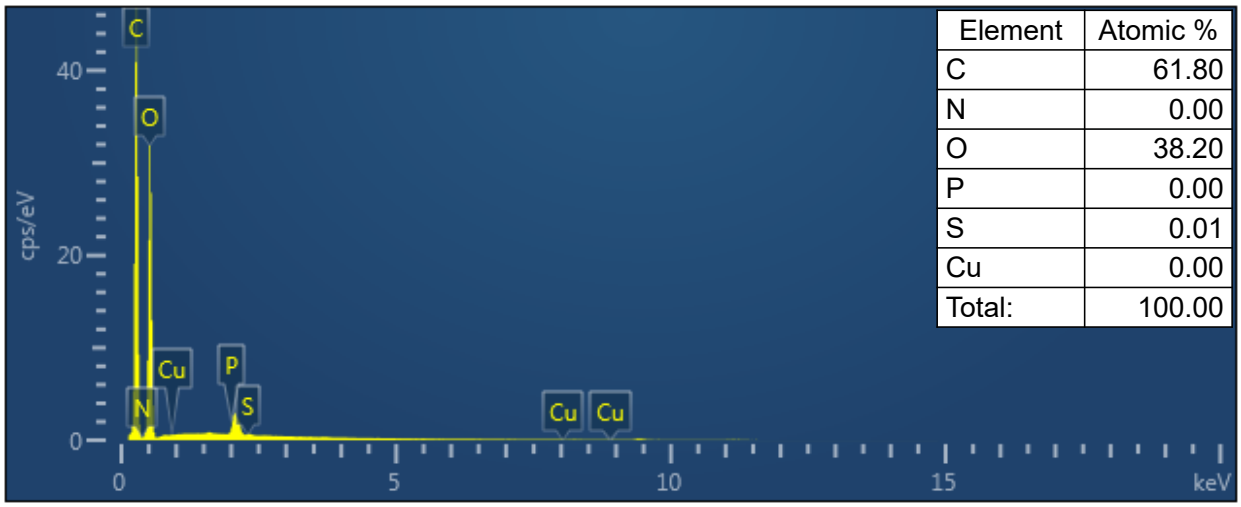

Element	Atomic %
C	61.80
N	0.00
O	38.20
P	0.00
S	0.01
Cu	0.00
Total:	100.00

Fig. S3 EDS spectrum and percentage atomic compositions of elements on the surface of a bare paper strip.

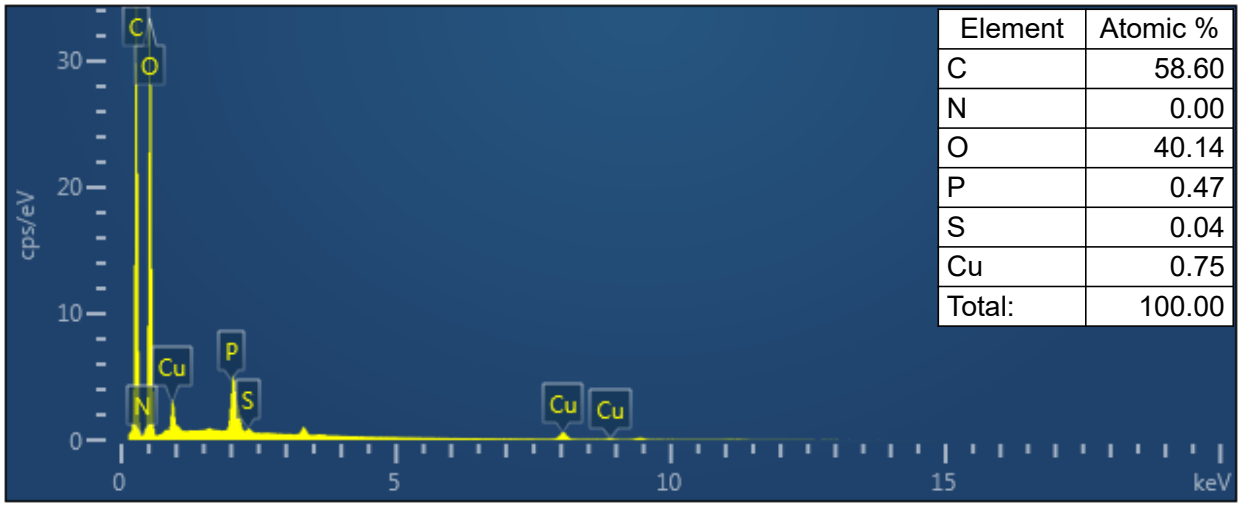

Element	Atomic %
C	58.60
N	0.00
O	40.14
P	0.47
S	0.04
Cu	0.75
Total:	100.00

Fig. S4 EDS spectrum and percentage atomic compositions of elements on the surface of paper strip deposited with $Cu_3(PO_4)_2.3H_2O$ nanoparticles.

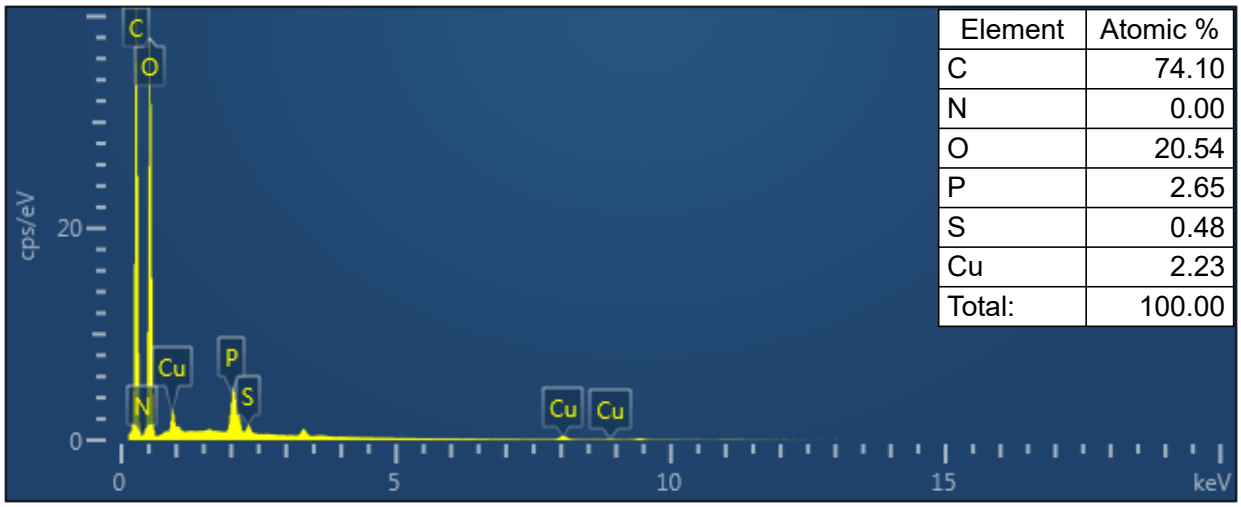

Element	Atomic %
C	74.10
N	0.00
O	20.54
P	2.65
S	0.48
Cu	2.23
Total:	100.00

Fig. S5 EDS spectrum and percentage atomic compositions of elements in the situ grown GOx&HRP@$Cu_3(PO_4)_2.3H_2O$ hybrid nanoflowers on of paper strip's surface.

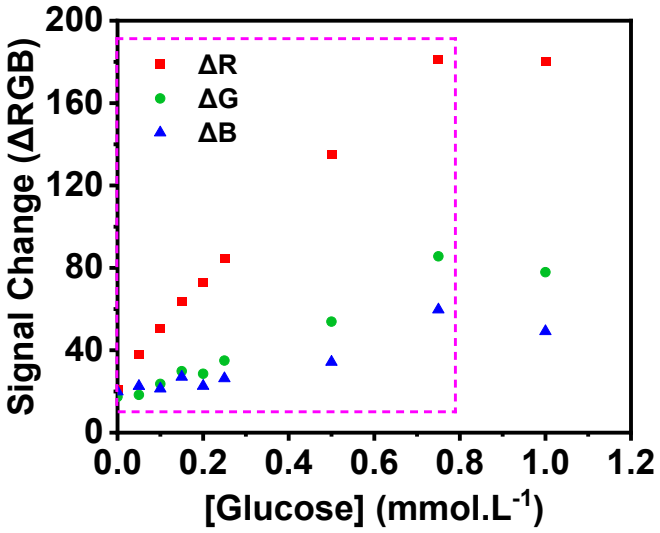

Fig. S6 Glucose detection using a fully assembled hybrid µDip sensor. The graph illustrating linear relationship between colorimetric signals and glucose concentration (0–1 $\boldsymbol{mmol\ L^{-1}}$), with the boxed region highlighting the region of strong linearity.

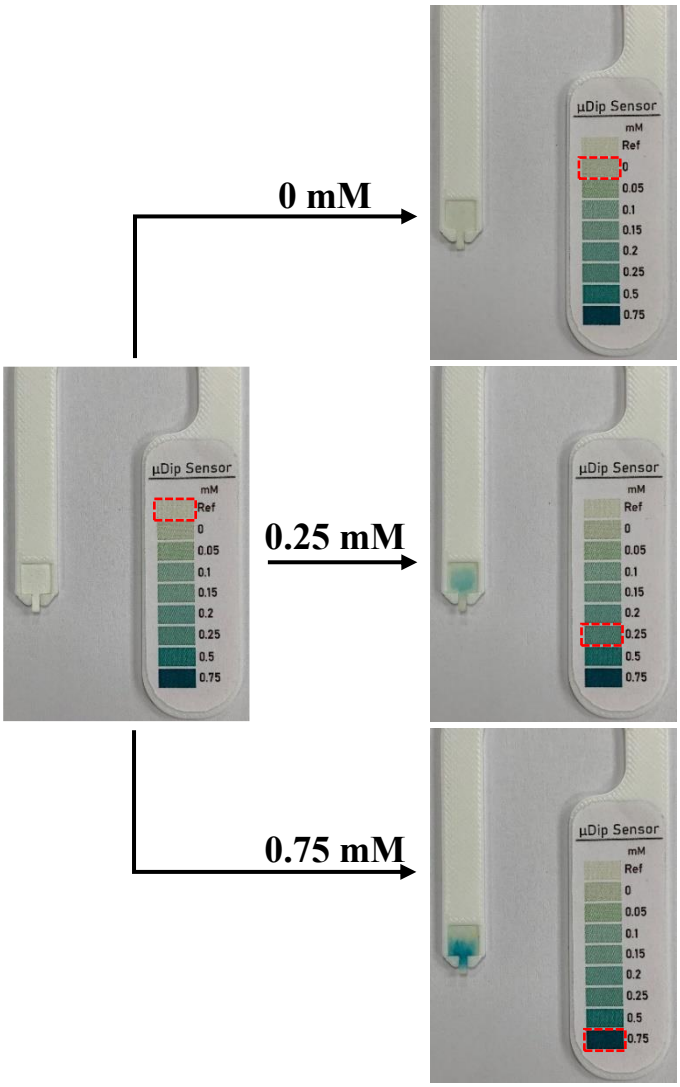

Fig. S7 Visual readout demonstration using three different concentrations of glucose.

The semi-quantitative visual detection capability of the hybrid µDip sensor, enabled by an integrated color reference chart with a 9-level colorimetric gradient (including reference level and 0–0.75 mmol/L glucose).

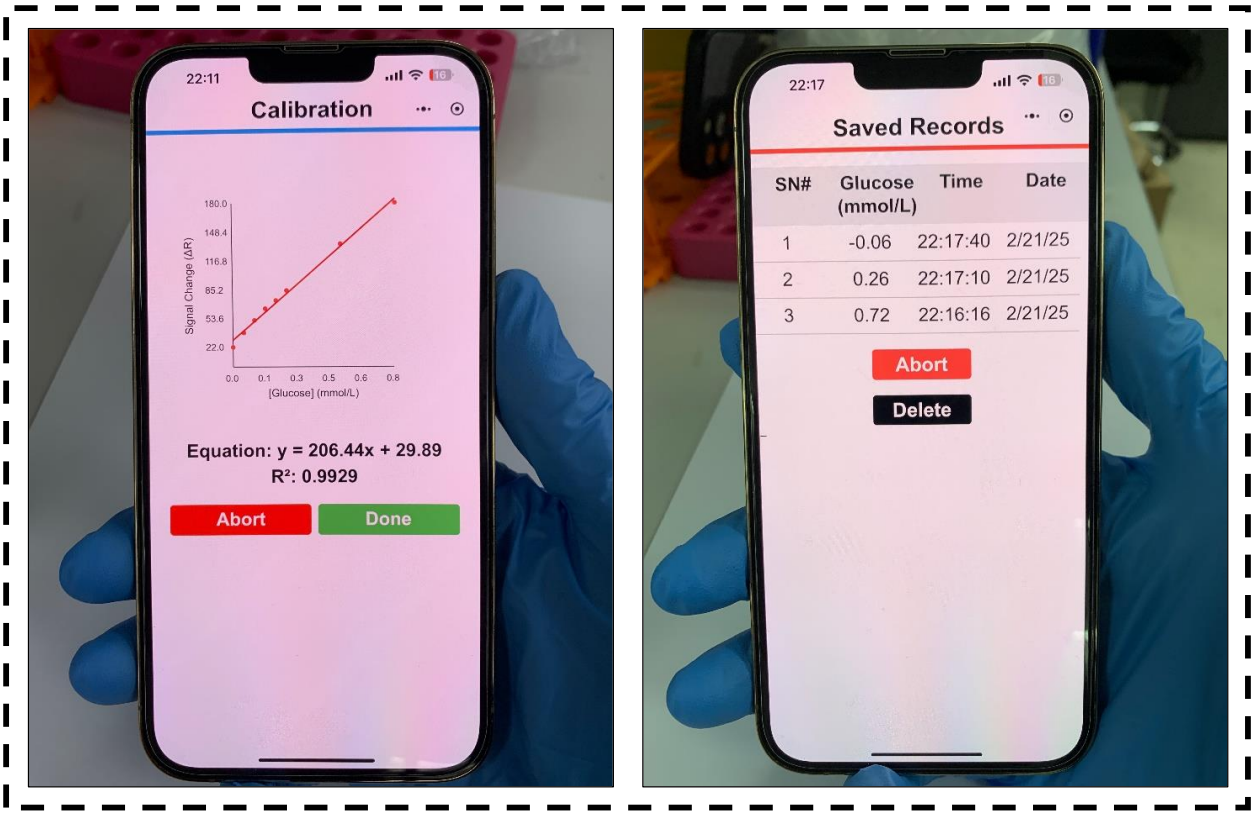

Fig. S8 Smartphone-based app calibration and validation of visual estimates. It shows the calibration curve demonstrating the linear response of the hybrid µDip sensor across the physiological urine glucose range (0-0.75 mmol/L), and validation of visual estimates from Fig. S7 showing digital readouts for the three standard samples.

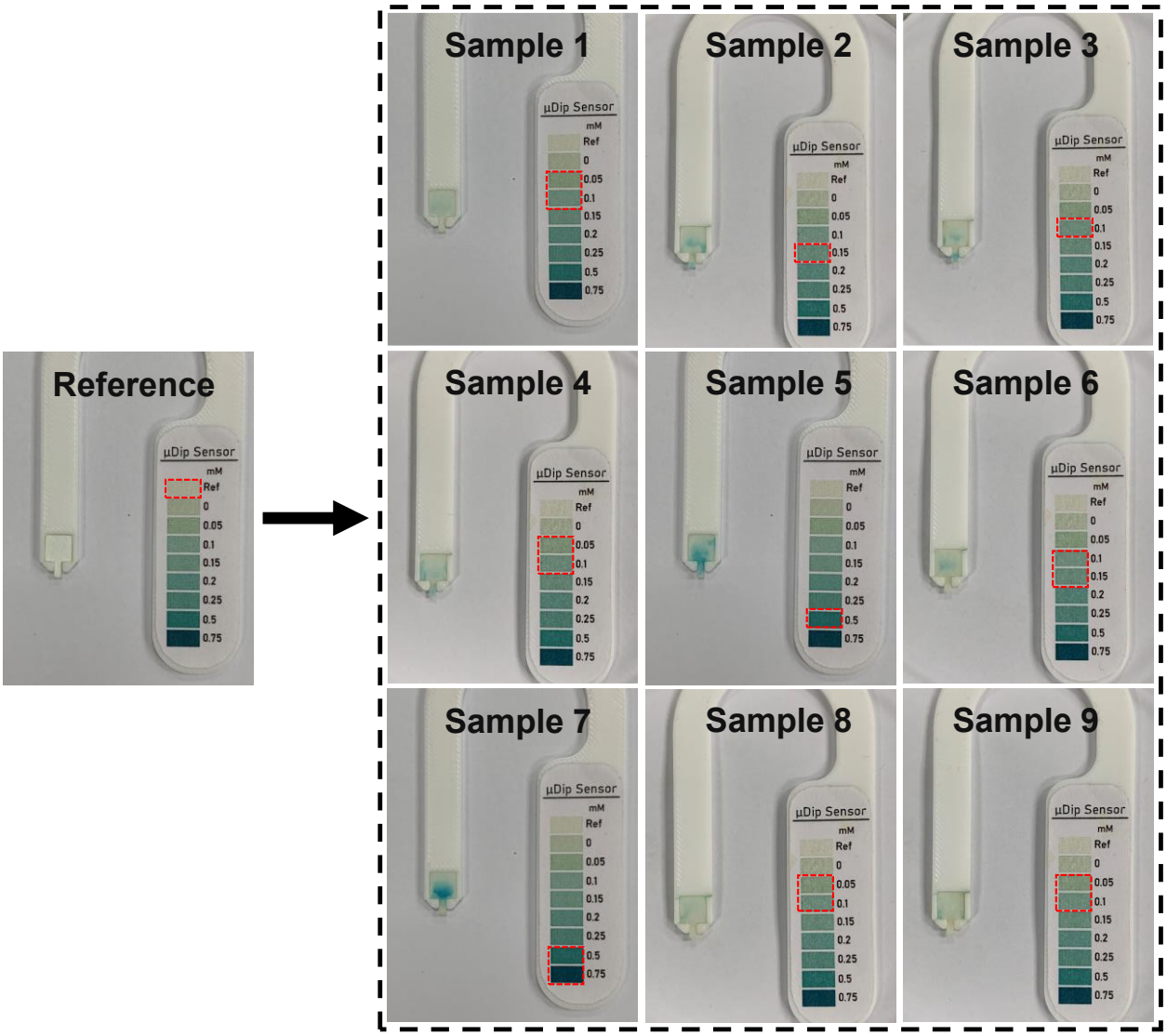

Fig. S9 Visual detection of urinary glucose using the hybrid µDip sensor. Colorimetric responses of nine urine samples (S1–S9) after reaction with the sensor, compared to a reference chart (0–0.75 mmol/L glucose in 0.05–0.25 mmol/L increments). Red boxes demarcate the best-matched reference concentration for each sample. Samples with exact matches (e.g., S2, S3, S5) align with single reference levels, while intermediate responses (e.g., S1, S4, S7–S9) fall between two adjacent reference colors, reflecting the sensor's semi-quantitative resolution.

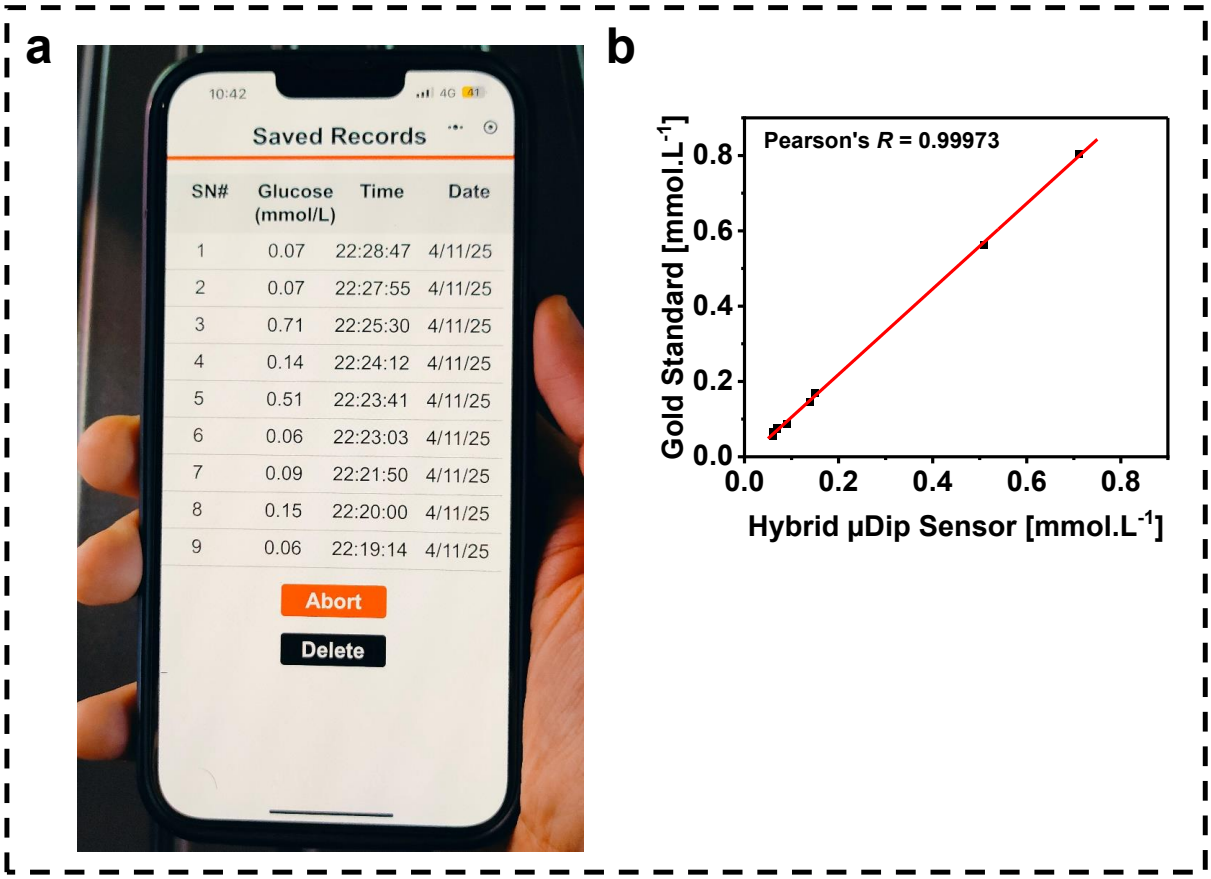

Fig. S10 Smartphone-based quantitative detection of urinary glucose using the hybrid µDip sensor. a Shows the saved records from smartphone app, displaying the quantitative glucose values of the 9 urine samples in a reverse chronological order (sample 9 – 1) as detected using the hybrid µDip sensor, which validate the visual estimates in Fig. S9. **b** Linear regression analysis comparing urine glucose quantification between the hybrid µDip sensor and the gold standard method.

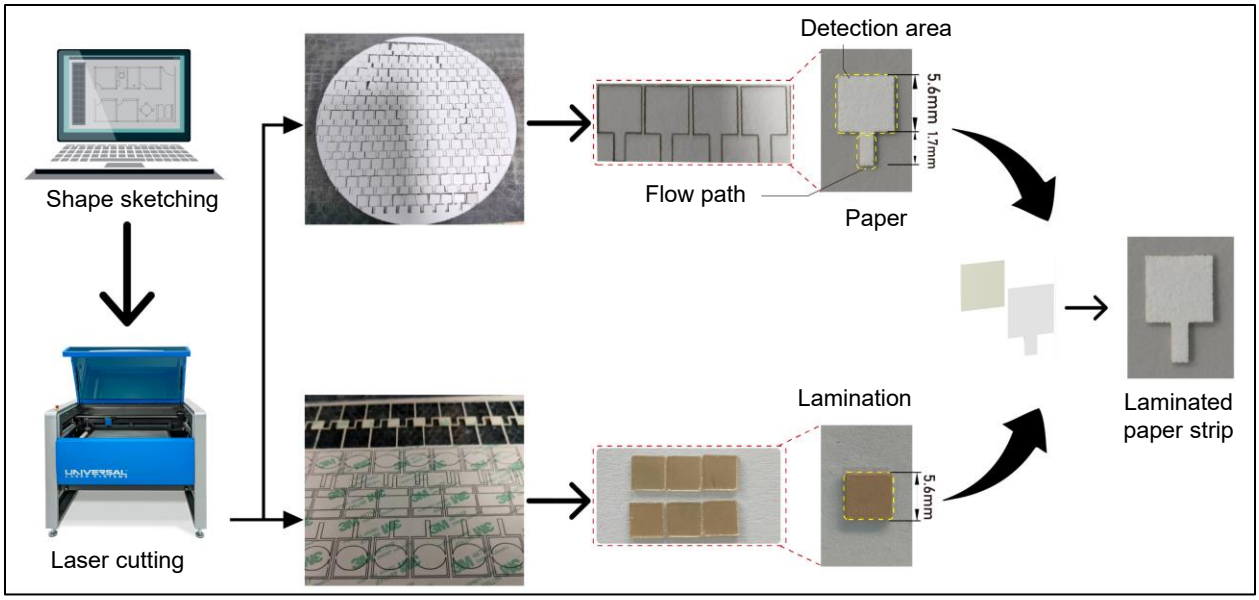

Fig. S11 Design, fabrication, and assembly process of the paper-strip for the hybrid µDip Sensor. The upper flow path illustrates the paper sketching and cutting process, while the lower flow path represents the lamination cutting process. Both components are ultimately adhered together to form the final laminated paper strip.

Table S1. Comparison of fluid transport efficiency between extruded-lamination (EL) and square-lamination (SL) paper strips in the hybrid µDip sensor.

Test Repeats	Paper strip with extruded lamination (EL)			Paper strip with square lamination (SL)		
	Distance Traveled (mm)	Time Taken (s)	Flow Rate (mm/s)	Distance Traveled (mm)	Time Taken (s)	Flow Rate (mm/s)
1	7.3	210	0.035	7.3	13	0.562
2	7.3	230	0.032	7.3	18	0.406
3	7.3	220	0.033	7.3	17	0.429
4	7.3	175	0.042	7.3	18	0.406
5	7.3	140	0.052	7.3	20	0.365
MEAN:			**0.039**			**0.433**
SD:			**0.008**			**0.027**
RSD:			**20.51%**			**6.24%**

Table S2. Comparison of glucose concentrations measured by the µDip sensor and the glucose oxidase reference assay with corresponding percent recovery values for urine samples.

Urine Sample	µDip-Sensor (mmol L^{-1})	Gold-Standard (mmol L^{-1})	% Recovery (%)	% Error (%)	|%Error| (%)
S1	0.06	0.06	92.33	7.67	7.67
S2	0.15	0.17	88.49	11.51	11.51
S3	0.09	0.09	104.29	-4.29	4.29
S4	0.06	0.06	108.15	-8.15	8.15
S5	0.51	0.56	90.62	9.38	9.38
S6	0.14	0.14	96.64	3.36	3.36
S7	0.71	0.80	88.43	11.57	11.57
S8	0.07	0.07	94.63	5.37	5.37
S9	0.07	0.08	92.70	7.30	7.30

Mean % Recovery = 95.14% ± 6.9%

Mean % Error (Bias) = −4.86%

MAPE = 7.62%

Movie S1. Assembly of the hybrid μDip sensor and preparation for glucose detection. Demonstrates placement of the hybrid nanoflowers functionalized paper strip into the microfluidic dipstick and taking the reference picture with smartphone prior to glucose reaction.

Movie S2. Simplified pre-addition of TMB drop using disposable dropper to prepare sample for dip-and-detect mechanism.

Movie S3. The dip-and-detect mechanism of the hybrid μDip sensor and real-time glucose quantification using a smartphone.